KYUNGPOOK Math. J. 61(2021), 831-843
https://doi.org/10.5666/KMJ.2021.61.4.831
pISSN 1225-6951 eISSN 0454-8124

The Effect of Slip on the Convective Instability Characteristics of the Stagnation Point Flow Over a Rough Rotating Disk

Dip Mukherjee* and Bikash Sahoo
Department of Mathematics, National Institute of Technology Rourkela, Rourkela-769008, Odisha, India
e-mail : 518ma1001@nitrkl.ac.in *and* bikashsahoo@nitrkl.ac.in

Abstract. In this paper we look at the three dimensional stagnation point flow problem over a rough rotating disk. We study the theoretical behaviour of the stagnation point flow, or forced flow, in the presence of a slip factor in which convective instability stationary modes appear. We make a numerical investigation of the effects of slip on the behaviour of the flow components of the stagnation point flow where the disk is rough. We provide, for the first time in the literature, a complete convective instability analysis and an energy analysis. Suitable similarity transformations are used to reduce the Navier-Stokes equations and the continuity equation into a system of highly non-linear coupled ordinary differential equations, and these are solved numerically subject to suitable boundary conditions using the *bvp4c* function of **MATLAB**. The convective instability analysis and the energy analysis are performed using the Chebyshev spectral method in order to obtain the neutral curves and the energy bars. We observe that the roughness of the disk has a destabilising effect on both Type-I and Type-II instability modes. The results obtained will be prominently treated as benchmarks for our future studies on stagnation flow.

1. Introduction

The classical problem of steady laminar flow caused due to the rotation of an infinite circular disk in a fluid at rest was first studied by Von Kármán [10], who discovered that the Navier-Stokes equations possess an exact solution. Rotating disk boundary-layer flow problems have been considered by engineers and scientists for past few decades due to their wide practical applications in thermal power generating systems, rotating machinery, medical equipment, computer storage devices,

* Corresponding Author.
Received April 22, 2020; revised November 29,2020; accepted November 30, 2020.
2010 Mathematics Subject Classification: 76D05.
Key words and phrases: Stagnation point flow, Chebyshev spectral method, Slip, Convective instability, Energy analysis.
This work was supported by Prof. Bikash Sahoo.

gas turbine rotors, air cleaning machines, crystal growth processes and most importantly aerodynamic applications. The main concern of our present study is three dimensional steady laminar stagnation point flow over a rotating disk, when the disk is rough.

The stagnation point flow is one of the major problems which we encounter with in many applications in the field of aerodynamics and in many flow fields in engineering. The seminal book by Schlichting [15] gives extenssive background on stagnation flow and its dynamics. Hiemenz [6] first formulated the problem, which describes two-dimensional stagnation flow directed orthogonally towards an infinite flat plate. He derived an exact solution to the Navier-Stokes equations. This problem later was extended to the case of axisymmetric flow by Homann [7]. The work of Homann was then extended by Hannah [8], who introduced axisymmetric stagnation flow against a rotating disk. Wang [17], in his study, stated that the stagnation region is where highest pressure, the highest heat transfer, and the highest level of mass deposition occur.

In most of the studies of fluid mechanics, the no-slip boundary condition is applied, assuming that the fluid adheres to a solid boundary. But in some cases like emulsions, suspensions, foams and polymer solutions [16], the no-slip condition is not adequate. In the case of a slip condition, the Navier-Stokes equations and the continuity equation can still be used together with a velocity slip factor in the boundary condition. Miklavačič and Wang [12] first extended the Von Kármán rotatng disk flow problem by considering that the lower disk admits partial slip due to having a rough surface. Later, Sahoo [14] investigated the effect of partial slip, viscous dissipation and joule heating on Von Kármán flow and heat transfer of an electrically conducting non-Newtonian fluid. Recently, Lingwood and Garrett [11] and Alveroglu et al. [1] introduced Coriolis force in the Navier-Stokes equations and studied its effects on the convective instability characteristics of the BEK family of flows rotating over a rough disk. They also established that anisotropic surface roughness has a stabilising effect on the instabilities within BEK family of flows (see Ref. [11, 1]).

In the above surveyed literature, the effect of slip on the convective instability characteristics of the stagnation point flow over a rough rotating disk was never considered. In this paper, we extend the work of Alveroglu et al. [1] to the case of stagnation point flow or forced flow over a rough rotating disk by considering a velocity slip factor in the boundary condition. A system of highly nonlinear differential equations representing the motion of the fluid is solved in order to obtain the velocity profiles. Also, a convective instability analysis and an energy analysis are performed to get the neutral curves and the energy bars by using the Chebyshev spectral method [18].

The structure of the paper is as follows. A brief description of the dynamics of stagnation flow is described and the Navier-Stokes equations together with the perturbation equations and the energy balance equation is formulated in Section 2. The results including the mean flow profiles, neutral curves and the energy bars along with the numerical results are presented in Section 3. Finally, we give

conclusions and motivations for our work.

2. Formulation of the Problem

2.1. The steady mean flow analysis

Stagnation point flow describes a flow of a viscous fluid in the immediate vicinity of a solid surface in which the fluid approaching the surface divides into different streams. Here, the stagnation point is the point of contact of the fluid with the solid surface. Here, the fluid velocity is zero. The governing equations of motion of the flow are derived from the generalized flow problem.

The dimensional Navier-Stokes equations and the continuity equation in cylindrical coordinate system (r^*, θ, z^*) are given by:

$$U^*_{t^*} + \overline{U}^* \cdot \nabla U^* - \frac{V^{*2}}{r^*} = -\frac{1}{\rho^*} P^*_{r^*} + \nu^* (\nabla^2 U^* - \frac{U^*}{r^{*2}} - \frac{2}{r^{*2}} V^*_\theta) \tag{2.1}$$

$$V^*_{t^*} + \overline{U}^* \cdot \nabla V^* + \frac{U^* V^*}{r^*} = -\frac{1}{\rho^* r^*} P^*_\theta + \nu^* (\nabla^2 V^* - \frac{V^*}{r^{*2}} + \frac{2}{r^{*2}} U^*_\theta) \tag{2.2}$$

$$W^*_{t^*} + \overline{U}^* \cdot \nabla W^* = -\frac{1}{\rho^*} P^*_{z^*} + \nu^* \nabla^2 W^* \tag{2.3}$$

$$U^*_{r^*} + \frac{U^*}{r^*} + \frac{1}{r^*} V^*_\theta + W^*_{z^*} = 0 \tag{2.4}$$

Here $\overline{\mathbf{U}}^* = (U^*, V^*, W^*)$ is the dimensional velocity field, ρ^* is the fluid density, P^* is the pressure, ν^* is the kinematic viscosity and t^* is time. Also, the flow is assumed to be axisymmetric and steady so that $\frac{\partial}{\partial \theta} \equiv 0$ and $\frac{\partial}{\partial t^*} \equiv 0$. The suitable boundary conditions subject to slip condition are introduced as:

$$\begin{gathered} U^* = \frac{2 - \xi_{V^*}}{\xi_{V^*}} \eta \frac{\partial U^*}{\partial z},\ V^* = \Omega r + \frac{2 - \xi_{V^*}}{\xi_{V^*}} \eta \frac{\partial V^*}{\partial z},\ W^* = 0 \\ U^* \to {U_e}^*,\ V^* \to {V_e}^*\ \ as\ \ z \to \infty \end{gathered} \tag{2.5}$$

where ξ_{V^*} is the tangential momentum accommodation coefficient, which is determined empirically (see Ref. [13]) and depends on the fluid and surface finish, η is the mean free path, and Ω is the rotation rate of the lower disk. For the case of a frictionless potential flow it is found that:

$${U_e}^* = a r^*,\ {V_e}^* = 0,\ {W_e}^* = -2 a z^*,\ P^* = -\frac{1}{2} \rho a^2 (r^{*2} + 4 z^{*2}) + P_0 \tag{2.6}$$

where a is a constant and P_0 is the stagnation pressure. Here, the stagnation point occurs at the origin O.

Let us consider the self-similarity of variables following Freidoonimehr *et al.* [4]. Taking the boundary-layer thickness $z = \sqrt{\frac{a}{\nu^*}}z^*$ as follows,

$$\begin{aligned} U^* = ar^*U(z), V^* = ar^*V(z), \\ W^* = \sqrt{a\nu^*}W(z), P^* = -\frac{1}{2}\rho a^2(r^2 + P(z)) \end{aligned} \tag{2.7}$$

and assuming $\frac{\partial}{\partial\theta} \equiv 0$ and $\frac{\partial}{\partial t^*} \equiv 0$, the Navier-Stokes equations and the continuity equation (2.1) - (2.4) become:

$$\frac{d^2U(z)}{dz^2} - W(z)\frac{dU(z)}{dz} - (U(z))^2 + (V(z))^2 + 1 = 0 \tag{2.8}$$

$$\frac{d^2V(z)}{dz^2} - W(z)\frac{dV(z)}{dz} - 2U(z)V(z) = 0 \tag{2.9}$$

$$\frac{dW(z)}{dz} + 2U(z) = 0 \tag{2.10}$$

where the non-dimensional variables U, V, W are the radial, azimuthal and axial velocity components respectively and P is the pressure in z. Now, the corresponding boundary conditions given by (2.5) and (2.6) are expressed in terms of the self-similarity variables in the following manner :

$$\begin{aligned} U(0) = \tilde{\gamma}U'(0),\ V(0) = \tilde{\omega} + \tilde{\gamma}V'(0),\ W(0) = 0 \\ U(z) \to 1,\ V(z) \to 0\ \ as\ \ z \to \infty \end{aligned} \tag{2.11}$$

where $\tilde{\gamma} = [(2-\xi_{V^*})\eta\sqrt{\frac{a}{\nu^*}}]/\xi_{V^*}$ is the slip factor and $\tilde{\omega} = \frac{\Omega^*}{a}$ represents the strength of rotation.

2.2. The perturbation equations

The perturbation equations are derived in order to perform a local stability analysis of the flow in the immediate vicinity of the lower disk. In this case, this is conducted in the boundary-layer adjacent to the stagnation point. The perturbation equations are formulated using the dimensional Navier-Stokes equations and the continuity equation (2.1) - (2.4), which are non-dimensionalised by the following local similarity variables:

$$\begin{aligned} U(z) = \frac{U^*}{ar_b^*\Omega^*}, V(z) = \frac{V^*}{ar_b^*\Omega^*}, W(z) = \frac{W^*}{ar_b^*\Omega^*}, \\ P(r,z) = \frac{P^*}{a^2\rho^*(r_b^*)^2(\Omega^*)^2}, t = \frac{t^*}{\frac{l^*}{ar_b^*\Omega^*}}, r = \frac{r_b^*}{l^*}, \end{aligned} \tag{2.12}$$

where $r_b{}^*$ is the local radial position of the disk and $l^* = \sqrt{\frac{\nu^*}{a\Omega^*}}$ is the boundary layer thickness. The non-dimensional Reynolds number is given by

$$Re = \frac{ar_b^*\Omega^* l^*}{\nu^*} = r \tag{2.13}$$

In order to derive the perturbation equations, the perturbed quantities are taken as:

$$\begin{aligned}
\tilde{u}(\tilde{\mathbf{x}},t) &= \frac{r}{Re}U(z) + u(\tilde{\mathbf{x}},t)\\
\tilde{v}(\tilde{\mathbf{x}},t) &= \frac{r}{Re}V(z) + v(\tilde{\mathbf{x}},t)\\
\tilde{w}(\tilde{\mathbf{x}},t) &= \frac{1}{Re}W(z) + h(\tilde{\mathbf{x}},t)\\
\tilde{p}(\tilde{\mathbf{x}},t) &= \frac{1}{Re^2}P(z) + p(\tilde{\mathbf{x}},t),
\end{aligned} \tag{2.14}$$

where $\tilde{\mathbf{x}} = (r,\theta,z)$ and $u,\ v,\ w,\ p$ are perturbed quantities.

Using the transformations (2.12) and (2.14) in the system of equations (2.1) - (2.4), the resulting linearised perturbation equations are given by:

$$\begin{aligned}
&u_t + \frac{rU}{Re}u_r + \frac{U}{Re}u + \frac{V}{Re}u_\theta + \frac{W}{Re}u_z - \frac{2V}{Re}v + \frac{r}{Re}\frac{dU}{dz}w\\
&= -p_r + \frac{1}{Re}(u_{rr} + \frac{1}{r^2}u_{\theta\theta} + u_{zz} + \frac{1}{r}u_r - \frac{u}{r^2} - \frac{2}{r^2}v_\theta)
\end{aligned} \tag{2.15}$$

$$\begin{aligned}
&v_t + \frac{rU}{Re}v_r + \frac{U}{Re}v + \frac{V}{Re}v_\theta + \frac{W}{Re}v_z + \frac{2V}{Re}u + \frac{r}{Re}\frac{dV}{dz}w\\
&= -\frac{1}{r}p_\theta + \frac{1}{Re}(v_{rr} + \frac{1}{r^2}v_{\theta\theta} + v_{zz} + \frac{1}{r}v_r - \frac{v}{r^2} + \frac{2}{r^2}u_\theta)
\end{aligned} \tag{2.16}$$

$$\begin{aligned}
&w_t + \frac{rU}{Re}w_r + \frac{1}{Re}\frac{dW}{dz}w + \frac{V}{Re}w_\theta + \frac{W}{Re}w_z\\
&= -p_z + \frac{1}{Re}(w_{rr} + \frac{1}{r^2}w_{\theta\theta} + w_{zz} + \frac{1}{r}w_r)
\end{aligned} \tag{2.17}$$

$$u_r + \frac{u}{r} + \frac{1}{r}v_\theta + w_z = 0 \tag{2.18}$$

In the above process of linearisation, the terms of $O(\frac{Ro^2}{Re^2})$ are neglected. Also, the second derivatives of the mean flow components i.e. $\frac{rRo}{Re}\frac{d^2U}{dz^2}$, $\frac{rRo}{Re}\frac{d^2V}{dz^2}$ and $\frac{Ro}{Re}\frac{d^2W}{dz^2}$ are ignored (see Ref. [1]). Now, the perturbed quantities are expanded on following Gustavasson [5], to carry out a normal mode analysis, as follows:

$$(u,v,w,p) = (\hat{u}(z),\hat{v}(z),\hat{w}(z),\hat{p}(z))e^{i(\alpha r + \overline{\beta}\theta - i\omega t)}. \tag{2.19}$$

Since, we are interested in the spatial analysis of the flow, it is assumed that $\alpha = \alpha_r + i\alpha_i \in \mathbb{C}$ is the radial wavenumber, $\overline{\beta} = \beta Re \in \mathbb{R}$ is the azimuthal wavenumber and $\omega \in \mathbb{R}$ is the frequency. Furthermore, $\overline{\beta}$ is assumed to be $O(1)$.

In order to separate the variables $r,\ \theta\ , z\ and\ t$, a parallel-flow approximation has been introduced. Therefore, the variable r has been replaced by $\frac{Re}{Ro}$. Therefore, the resulting separable linearised perturbation equations are

$$-\frac{1}{Re}\frac{d^2\hat{u}}{dz^2} + \frac{1}{Re}W\frac{d\hat{u}}{dz} + (i\alpha U + i\beta V - i\omega + \frac{\alpha^2}{Re} + \frac{\beta^2}{Re} + \frac{1}{Re}U)\hat{u} - \frac{2}{Re}V\hat{v} + \frac{dU}{dz}\hat{w} + i\alpha\hat{p} = 0 \tag{2.20}$$

$$-\frac{1}{Re}\frac{d^2\hat{v}}{dz^2} + \frac{1}{Re}W\frac{d\hat{g}}{dz} + (i\alpha U + i\beta V - i\omega + \frac{\alpha^2}{Re} + \frac{\beta^2}{Re} + \frac{1}{Re}U)\hat{v} + \frac{2}{Re}V\hat{u} + \frac{dV}{dz}\hat{w} + i\beta\hat{p} = 0 \tag{2.21}$$

$$-\frac{1}{Re}\frac{d^2\hat{w}}{dz^2} + \frac{1}{Re}W\frac{d\hat{w}}{dz} + (i\alpha U + i\beta V - i\omega + \frac{\alpha^2}{Re} + \frac{\beta^2}{Re} + \frac{1}{Re}\frac{dW}{dz})\hat{w} + \hat{p} = 0 \tag{2.22}$$

$$(i\alpha + \frac{1}{Re})\hat{u} + i\beta\hat{v} + \frac{d\hat{w}}{dz} = 0 \tag{2.23}$$

Here, the terms of order $(\frac{Ro}{Re})^2$ and $\frac{1}{Re^2}$ are neglected. Following the analysis by Cooper et al. [2], the perturbation quantities have to be zero near the surface of the disk to satisfy the slip condition. Also, the continuity equation (2.23) implies that $\frac{d\hat{w}}{dz}(z) = 0$ should be zero at the disk surface. Furthermore, the perturbation quantities at the far end of the disk should also be zero to ensure that the disturbances are confined within the boundary-layer. Therefore, the relevant boundary conditions are:

$$\hat{u}(z) = \hat{v}(z) = \hat{w}(z) = \frac{d\hat{w}}{dz}(z) = \hat{p}(z) = 0\ at\ z = 0 \tag{2.24}$$

$$\hat{u}(z) \to 0, \hat{v}(z) \to 0, \hat{w}(z) \to 0, \hat{p}(z) \to 0\ as\ z \to \infty. \tag{2.25}$$

Since we are interested in finding the stationary modes, we will assume that the frequency ω is 0 throughout our calculations. It is observed that our present analysis is consistent with Cooper et al. [2].

2.3. The energy balance equation

A useful method for examining the stability of an initial perturbation is by calculating its kinetic energy in the volume of the boundary-layer. Here, we perform

a spatial stability analysis by calculating the kinetic energy equation of the perturbation equation, which was first introduced by Cooper and Carpenter [3]. The linearised perturbation Eqs. (2.20) - (2.23) are multiplied by the perturbation quantities $\hat{u}, \hat{v}, \hat{w}$ and $\hat{p}$ respectively. Then the obtained equations are added to derive the kinetic energy equation in u,v,w and p, which is given by:

$$\begin{aligned}(\frac{\partial}{\partial t}+U\frac{\partial}{\partial r}+\frac{V}{Re}\frac{\partial}{\partial\theta}+\frac{W}{Re}\frac{\partial}{\partial z})K=\\ -uw\frac{dU}{dz}-vw\frac{dV}{dz}-\frac{1}{Re}w^2\frac{dW}{dz}+\frac{U}{Re}u^2+\frac{U}{Re}v^2\\ -[\frac{\partial}{\partial r}(up)+\frac{1}{Re}\frac{\partial}{\partial\theta}(vp)+\frac{\partial}{\partial z}(wp)+\frac{1}{Re}up]+[\frac{\partial}{\partial x_i}(u_j\sigma_{ij})-\sigma_{ij}\frac{\partial u_j}{\partial x_i}]\end{aligned} \tag{2.26}$$

Here, $\sigma_{ij}=\frac{1}{Re}[\frac{\partial u_i}{\partial x_j}+\frac{\partial u_j}{\partial x_i}]$ is the stress tensor and $K=\frac{1}{2}(u^2+v^2+w^2)$.

Since it is assumed that the flow is steady and rotationally symmetric, the derivatives with respect to t and θ are negleted. Now, Eqn. (2.26) is integrated across the boundary-layer, which leads to the energy integral equation as follows:

$$\begin{aligned}\int_0^\infty[\underbrace{U\frac{\partial\overline{K}}{\partial r}}_{\text{a}}+\underbrace{\frac{\partial\overline{(up)}}{\partial r}}_{\text{b}}-\underbrace{\frac{\partial}{\partial r}(\overline{u\sigma_{11}}+\overline{v\sigma_{12}}+\overline{w\sigma_{13}})}_{\text{c}}]dz=\\ \underbrace{\int_0^\infty[(-\overline{uw}\frac{dU}{dz})+(-\overline{vw}\frac{dV}{dz})+(-\overline{w^2}\frac{1}{Re}\frac{dW}{dz})]}_{\text{I}}-\underbrace{\int_0^\infty(\overline{\sigma_{ij}\frac{\partial u_j}{\partial x_i}})}_{\text{II}}\\ \underbrace{-\int_0^\infty(\frac{1}{Re}\overline{up})dz+\overline{(wp)}_{\overline{W}}}_{\text{III}}+\underbrace{[\overline{u\sigma_{31}}+\overline{v\sigma_{32}}+\overline{w\sigma_{33}}]_{\overline{W}}}_{\text{IV}}\\ \underbrace{-\int_0^\infty\frac{1}{Re}\frac{\partial\overline{K}}{\partial z}+\int_0^\infty\frac{1}{Re}\overline{u^2}Udz+\int_0^\infty\frac{1}{Re}\overline{v^2}Udz}_{\text{V}}\end{aligned} \tag{2.27}$$

Overbars denote a period-averaged quantity such that $\overline{fg}=fg^*+f^*g$, where $*$ indicates a complex conjugate and $\overline{W}$ in the subscript denotes quantities calculated at the wall. Now the energy balance equation (2.27) is normalised to obtain:

$$\begin{aligned}-2\alpha_i=\underbrace{(P_1+P_2+P_3)}_{\text{I}}+\underbrace{D}_{\text{II}}+\underbrace{(PW_1+PW_2)}_{\text{III}}+\underbrace{(S_1+S_2+S_3)}_{\text{IV}}\\ +\underbrace{(G_1+G_2+G_3)}_{\text{V}}\end{aligned} \tag{2.28}$$

The quantities indicated in Equations (2.28) and (2.27) are as follows.
(a) term arising due to kinetic energy flow by the radial component,
(b) contributions from the work done by the perturbation pressure term,

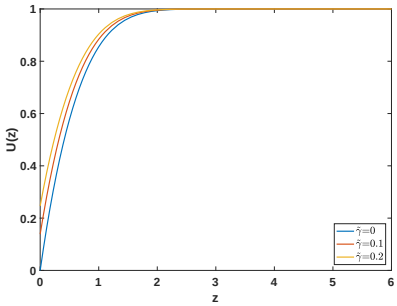

Figure 1: Flow component in the radial direction

(c) terms arising from the work done by the viscous stress quantity in the interior of boundary-layer,
(I) the Reynolds stress energy production terms, P_i's,
(II) the viscous dissipation energy removal term, D,
(III) contributions from the work done by the pressure terms, PW_i's,
(IV) contributions from the work done on the wall by the viscous stresses, S_i's,
(V) terms arising due to the streamline curvature effects and the three dimensional flow, G_i's.
The terms PW_2, S_1, S_2 and S_3 are identically equal to zero due to the boundary conditions (2.24) - (2.25).

3. Results and Discussions

3.1. The mean flow velocity profiles

The highly nonlinear and coupled similarity Eqs. (2.8) - (2.10) have been solved subject to the boundary conditions (2.11) taking $\tilde{\omega} = 1$. The velocity profiles for different values of the slip parameter $\tilde{\gamma}$ are computed by using the *bpv4c* function in **MATLAB** [9]. The following figures represent the velocity profiles of the stagnation point flow in the immediate vicinity of the wall of the lower disk.

Fig. 1 demonstrates the effect of slip $\tilde{\gamma}$ on the radial component of the flow for a specified value of the rotation strength parameter $\tilde{\omega}$. Now, if we look at the figure it is observed that as the value of $\tilde{\gamma}$ increases the radial velocity of the flow increases near the surface of the disk and gradually converges to its limiting value, but the radial velocity boundary-layer thickness is reduced. The above observation indicates the fact that less fluid is drawn and pushed away in the radial direction as the slip gets stronger. A decrease in the angular velocity with an increasing value of $\tilde{\gamma}$ near the surface of the disk is seen in Fig. 2. In this case also, the angular velocity boundary-layer thickness declines as the slip factor is increased. Fig. 3

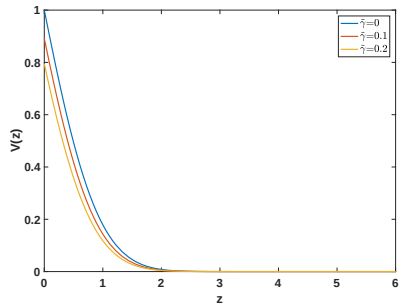

Figure 2: Flow component in the angular direction

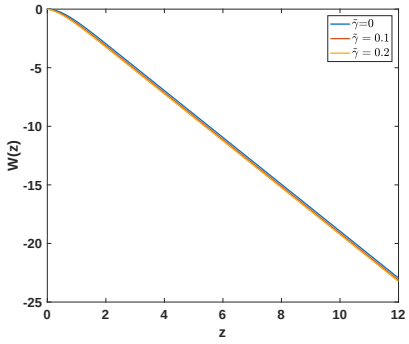

Figure 3: Flow component in the axial direction

demonstrates the axial component of the flow. A decrease in the axial velocity and reduction of the boundary-layer thickness occurs increasing $\tilde{\gamma}$. This is because as the slip gets stronger the fluid particles are pushed away in the radial direction and the fluid particles are attracted towards the negative axial direction. The Table 1 is given for future references.

$\tilde{\gamma}$	$F'(0)$	$-G'(0)$
0	1.5739	1.1010
0.1	1.3879	1.0836
0.2	1.2323	1.0274

Table 1: The numerical values of radial and tangential skin friction coefficient $F'(0)$ and $-G'(0)$ for different values of $\tilde{\gamma}$ at $\tilde{\omega} = 1$:

3.2. The neutral curves

A neutral curve encloses a region in the plane which represents an unstable region for the boundary layers. The upper lobe of a neutral curve represents inviscid Type-I mode whereas the lower lobe represents viscous Type-II mode. The main aim for obtaining the neutral curves is to determine whether slip has a stabilising or destabilising effect on the flow. The neutral curves are obtained by solving Eqs. (2.20)- (2.23) subject to the boundary conditions Eqs. (2.24)- (2.25) using the Chebyshev spectral method (see Ref. [18]) to compute the convective instability characteristics in terms of the neutral curves. The neutral curves are presented in the (Re, α_r)-plane.

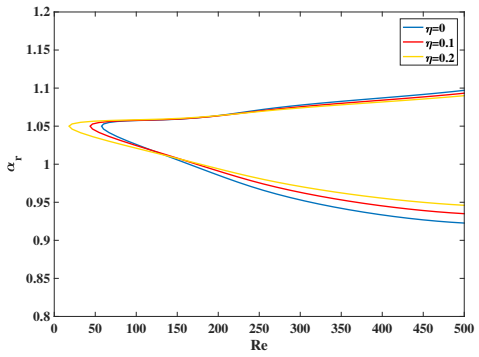

Figure 4: The neutral curves of stagnation point flow in (Re, α_r)-plane

Fig. 4 demonstrates neutral curves in (Re, α_r)-plane. Observe that the area of

the unstable region enclosed by the curves increases with the slip factor $\tilde{\gamma}$ for $\tilde{\omega} = 1$. This indicates the fact that roughness of the disk has a globally destabilising effect on the stationary Type-I and Type-II modes. The following table (Table 2) shows the critical values of Re.

$\tilde{\gamma}$	Re
0	57.71
0.1	43.76
0.2	18.04

Table 2: The critical values of Reynolds number Re for the onset of the convective instability for different values of $\tilde{\gamma}$ at $\tilde{\omega} = 1$:

3.3. The energy bars

The energy bars indicate the kinetic energy changes in the flow due to the induced perturbation in the system. The energy bars have been obtained by solving the corresponding energy integral equation of the perturbation equations. Here, the positive terms signify the energy production whereas negative terms remove energy from the system. An increasing energy change indicates a destabilisation effect whereas decreasing energy change indicates a stabilisation effect. In order to validate the result discussed in Subsection 3.2, an energy analysis has been done by solving the energy integral Equation. (2.28). In Fig. 5 it is seen that with increasing slip factor $\tilde{\gamma}$, the total kinetic energy **TE** of the rotating disk flow increases, i.e., the system shows a destabilising effect with increasing $\tilde{\gamma}$. This validates the result obtained in the previous subsection. This method of validation can be applied to any other rotating disk flow problems.

4. Conclusions

For the first time in the literature, the effect of slip on the convective instability characteristics of the stagnation flow has been considered. Suitable similarity transformations were used to reduce the Navier-Stokes equations and the continuity equation into a system of highly nonlinear coupled ordinary differential equations, and these solved numerically subject to suitable boundary conditions in order to get the velocity profiles. From the obtained results it was observed that with increasing values of $\tilde{\gamma}$ the radial velocity increases whereas the angular and axial velocity decreases. But the boundary-layer thickness of each velocity components decreased as the value of $\tilde{\gamma}$ was increased.

A convective instability analysis and an energy analysis were conducted using the Chebyshev spectral method in order to solve the perturbation equations and the energy balance equation, and to get the neutral curves and the energy bars respectively. A globally destabilising effect on the instability modes (both Type-I

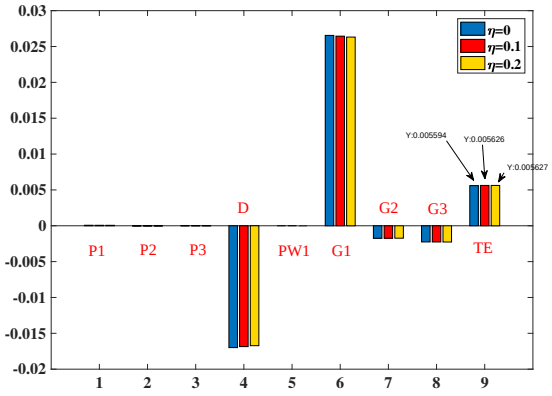

Figure 5: The energy bars indicating the kinetic energy change in the flow at $Re = Re_{critical}$

and Type-II) was observed with increasing slip factors i.e. as the value of $\tilde{\gamma}$ increased the instability of the flow began to increase. The results obtained in this paper will be treated as benchmarks in our future studies on stagnation flow.

Acknowledgments. The first author would like to thank the second author for his guidance and support, and the institute for financial support.

References

[1] B. Alveroglu, A. Segalini, S. J. Garrett, The effect of surface roughness on the convective instability of the bek family of boundary-layer flows, Eur. J. Mech. B Fluids, **56**(2016), 178–187.

[2] A. Cooper, J. Harris, S. J. Garrett,M. Özkan, P. Thomas, The effect of anisotropic and isotropic roughness on the convective stability of the rotating disk boundary layer, Phys. Fluids, **27**(2015), 014107.

[3] A. Cooper, P. W. Carpenter, The stability of rotating-disc boundary-layer flow over a compliant wall. part 1. type I and II instabilities, J. Fluid Mech., **350**(1997), 231–259.

[4] N. Freidoonimehr, M. M. Rashidi, S. Mahmud, F. Nazari, Slip effects on MHD stagnation point-flow and heat transfer over a porous rotating disk, Phys. Sci. Int. Jr., **5(1)**(2015), 34–50.

[5] L. H. Gustavsson, Initial-value problem for boundary layer flows, Phys. Fluids, **22**(1979), 1602–1605.

[6] K. Hiemenz, Die Grenzschicht an einem in den gleichformigen Flussigkeitsstrom eingetauchten geraden Kreiszylinder, Dinglers Polytech. J. **326**(1911), 321–324.

[7] F. Homann, Der Einfluss grosser Zähigkeit bei der Strömung um den Zylinder und um die Kugel, ZAMM-J. Appl. Math. Mech., **16(3)**(1936), 153–164.

[8] D. M. Hannah, Forced flow against a rotating disk, Rep. Mem. Aerosp. Res. Coun. Lond. 2772(1947).

[9] B. Hahn, D. Valentine, Essential MATLAB for engineers and scientists, Academic Press(2016).

[10] Th. von Kármán, Uber laminare und turbulente reibung, Z. Angew. Math. Mech., **1**(1921), 233–252.

[11] R. Lingwood, S. Garrett, The effects of surface mass flux on the instability of the bek system of rotating boundary-layer flows, Eur. J. Mech. B Fluids, **30**(2011), 299-310.

[12] M. Miklavačič, C. Y. Wang The flow due to a rough rotating disk, Zeitschrift für angewandte Mathematik und Physik ZAMP, **55**(2004), 235-246.

[13] M. Renksizbulut, H. Niazmand, G. Tercan, Slip-flow and heat transfer in rectangular microchannels with constant wall temperature, International Journal of Thermal Sciences, **45**(2006), 870-881.

[14] B. Sahoo, Effects of partial slip, viscous dissipation and Joule heating on Von Kármán flow and heat transfer of an electrically conducting non-Newtonian fluid, Communications in Nonlinear Science and Numerical Simulation, **14**(2009), 2982-2998.

[15] H. Schlichting, Boundary-layer Theory, McGraw-Hill, 1979.

[16] C. Y. Wang, Flow due to a stretching boundary with partial slip - an exact solution of the Navier-Stokes equations, Chem. Eng. Sci., **57**(2002), 3745-3747.

[17] C. Y. Wang, Stagnation flow on the surface of a quiescent fluid - An exact solution of the Navier-Stokes equations, Q. Appl. Math., **43(2)**(1985), 215-223.

[18] A. Zebib, A Chebyshev method for the solution of boundary value problems, J. Comput. Phys., **53**(1984), 443-455.